A UV study of nearby luminous infrared galaxies: star formation histories and the role of AGN

S. Kaviraj[1]*

[1] *Department of Physics, University of Oxford, Keble Road, Oxford, OX1 3RH, UK*

14 June 2013

ABSTRACT

We employ UV and optical photometry, from the GALEX and SDSS surveys respectively, to study the star formation histories (SFHs) of 561 luminous infrared galaxies ($L_{IR} > 10^{11}L_\odot$) in the nearby ($z < 0.2$) Universe. Visual inspection of a subsample of galaxies with $r < 16.8$ and $z < 0.1$ (for which eyeball classification of galaxy morphologies is reliable) indicates that a small fraction ($\sim 4\%$) have spheroidal or near-spheroidal morphologies and could be progenitors of elliptical galaxies. The remaining galaxies are morphologically late-type or ongoing mergers. 61% of the LIRGs do not show signs of interactions (at the depth of the SDSS images), while the remaining objects are either interacting ($\sim 18\%$) or show post-merger morphologies ($\sim 19\%$). Notwithstanding the high obscuration in their stellar continua ($< A(FUV) > \sim 2.6$ mags, assuming a Calzetti dust law), virtually all low-redshift LIRGs inhabit in the UV 'blue cloud'. The (SSP-weighted) *average* age of the underlying stellar populations in these objects is typically 5-9 Gyrs, with a mean value of ~ 6.8 Gyrs. $\sim 60\%$ of the LIRG population began their recent star formation (RSF) episode within the last Gyr, while the remaining objects began their RSF episodes 1 to 3 Gyrs in the past. Up to 35% of the stellar mass in the remnant forms in these episodes - the mean value is $\sim 15\%$. The (decay) timescales of the star formation are typically $\sim$few Gyrs, indicating that the star formation rate does not decline significantly during the course of the burst. 14% of the LIRG population host (Type 2) AGN, with a hint that the AGN fraction rises in interacting population (although low number statistics hamper a robust result). The AGN hosts show UV and optical colours that are redder than those of the normal (non-AGN) population. There is no evidence for a systematically higher dust content in the AGN hosts. AGN typically appear $\sim 0.5 - 0.7$ Gyrs after the onset of star formation and the redder colours are a result of older RSF episodes, *with no measurable evidence of negative feedback from the AGN on the star formation in their host galaxies.* Finally, we use the spheroidal and near-spheroidal objects identified in this sample to study the star formation that is plausibly induced by major mergers in the low redshift Universe. The spheroidal remnants exhibit (SSP-weighted) average ages of ~ 6.9 Gyrs and form between 5 and 30% of their stellar mass in the RSF episode, over time periods between 0.3 and 4 Gyrs. We speculate that these galaxies are the products of 'mixed' major mergers, where at least one of the progenitors has late-type morphology.

Key words: galaxies: evolution – galaxies: formation – galaxies: interactions – infrared: galaxies – ultraviolet: galaxies

1 INTRODUCTION

The first infrared (IR) all-sky survey, performed by the Infrared Astronomical Satellite (IRAS; Neugebauer et al. 1984), yielded a vast population of 'Luminous Infrared Galaxies' (LIRGs) that emit the bulk of their bolo-metric luminosity in the far-infrared (FIR) wavelengths (Sanders & Mirabel 1996). At luminosities greater than $\sim 10^{11}L_\odot$, they dominate the galaxy census in the nearby Universe, becoming more numerous (at comparable luminosities) than optically selected star-forming galaxies, Seyferts and quasi-stellar objects (QSOs) (Soifer et al. 1987; Soifer & Neugebauer 1991; Sanders & Mirabel 1996). Traditionally, a distinction is made between LIRGs, in which

* E-mail: skaviraj@astro.ox.ac.uk

$10^{11} L_\odot < L_{IR} < 10^{12} L_\odot$ and a more powerful class of 'Ultra-Luminous Infrared Galaxies' (ULIRGs) which satisfy $L_{IR} > 10^{12} L_\odot$.

The infrared continua of LIRGs is dominated by thermal re-radiation, by dust, of the ultra-violet (UV) flux from massive main sequence stars in regions of intense star formation activity, with a minor contribution from a dust-enshrouded AGN (e.g. Rowan-Robinson & Crawford 1989). While the role of the AGN may increase in significance for $L_{IR} > 10^{12} L_\odot$, the relative contributions from star formation and the AGN in ULIRGs are still a matter of some debate (see Joseph 1999; Sanders 1999; Elbaz et al. 2005; Teng et al. 2005, and references therein). While 'cool' ULIRGs ($f_{25}/f_{60} < 0.25$) may simply involve scaled up versions of the starbursts that drive LIRGs (e.g. Egami et al. 2004), a substantial AGN contribution to the infrared continuum is expected in 'warm' ULIRGS ($f_{25}/f_{60} > 0.25$), which exhibit optical, near-infrared and X-ray signatures of a powerful (dust-enshrouded) AGN (e.g. Veilleux et al. 1999; see Chakrabarti et al. 2007 for a theoretical interpretation).

The vigorous star formation activity itself is thought to be induced either by (molecular) gas-rich mergers (e.g. Sanders & Mirabel 1996; Sanders & Ishida 2004; Laag et al. 2006) or by bar-driven star formation in spiral galaxies (e.g. Wang et al. 2006). While the contributions to the LIRG population from mergers and spirals at the high mass end ($M_* > 10.5 M_\odot$) are comparable in the nearby Universe (Wang et al. 2006), ULIRGs are composed almost exclusively of objects that appear to be in the advanced stages of a major merger (e.g. Arp 220; Soifer et al. 1984; Sanders & Mirabel 1996). The merger-driven nature of both LIRGs and ULIRGs is consistent with the fact that both populations typically inhabit the field (e.g. Goto 2005; Zauderer et al. 2007), where relative velocities are lower and merging is more frequent.

The relative abundance of LIRGs shows a strong evolution with redshift, consistent with the steep decline of the cosmic star formation rate (SFR) that is observed over the last 8 billion years (Lilly et al. 1996; Madau et al. 1998). While they are relatively rare in the local Universe, comparison of the IR luminosity functions from IRAS, at $z < 0.3$, to surveys by the Infrared Space Observatory (ISO; Taniguchi et al. 1997; Elbaz1999) at intermediate redshifts ($0.3 < z < 1.5$) indicates that the comoving space density of LIRGs rises by approximately three orders of magnitude in the redshift range $0 < z < 1$ (Sanders 2003). The large population of faint submillimeter sources discovered using the SCUBA camera (e.g. Smail et al. 1997) provides access to the ULIRG population at $z >> 1$ (with the ULIRGs dominating the energy density in this redshift regime). These submillimeter studies (see e.g. Lilly et al. 1999), coupled with accurate determinations of the mean redshift of the submillimeter population (e.g. Chapman et al. 2003), indicate that the space density of ULIRGs at $z \sim 2.4$ is a factor of 10^3 higher than in the local Universe. Furthermore, their total FIR luminosity density exceeds the optical luminosity density from the general galaxy population by up to an order of magnitude at $z > 1.5$. Finally, morphological studies of LIRGs over the last 8 billion years indicate that the relative proportions of mergers and spirals evolve with redshift (Melbourne et al. 2005), with the fraction of mergers steadily increasing to-

wards present-day (e.g. Zheng et al. 2004; Bell et al. 2005; Wang et al. 2006).

The advent of the GALEX ultra-violet (UV) space telescope (Martin et al. 2005) is revolutionising our understanding of the local Universe in the UV wavelengths (shortward of $\sim 3000 Å$). The UV spectrum is overwhelmingly dominated by flux from young massive main sequence stars, making it an ideal probe of recent star formation (RSF) in a variety of systems. Furthermore, the UV remains largely unaffected by the age-metallicity degeneracy (Worthey 1994) that typically plagues optical analyses (Kaviraj et al. 2007a), making it an ideal photometric indicator of RSF. Among the many successes of the new GALEX results has been the detection of widespread low-level RSF in the nearby early-type population (see Kaviraj et al. (2007b) for a review) and new insights into the quenching mechanisms that operate in post-starburst (E+A) galaxies at low redshift (Kaviraj et al. 2007c).

Given its sensitivity to recent and ongoing star formation, the combination of UV and optical photometry is ideal for exploring the star formation histories (SFHs) of the nearby LIRG population. GALEX data has already been employed in the study of LIRGs and its evolution with redshift. Burgarella et al. (2005a) studied the GALEX photometry of 19 galaxies with spectroscopic redshifts that are observed at $15\mu m$ as part of the European Large-Area ISO Survey (ELAIS). The objects selected exhibit infrared luminosities in the range $10^{10} L_\odot < L_{IR} < 10^{13} L_\odot$ and most are in the nearby Universe ($z < 0.3$). Comparison of their IR and UV luminosities yields an average dust attenuation in the FUV ($\sim 1530 Å$) of $A(FUV) \sim 2.7$ mags (see also Burgarella et al. 2005b). A recent study of 190 intermediate-redshift ($z \sim 0.7$) LIRGs, observed with Spitzer/MIPS and GALEX (Buat et al. 2007), reveals that the dust attenuation (as traced by L_{IR}/L_{UV}) in these objects remains moderate to these redshifts ($A_{FUV} < 3$ mags), with a slight decrease in the mean FUV dust attenuation of ~ 0.5 mag in the redshift range $0 < z < 0.7$, plausibly driven by lower metallicities and an increase in the proportion of spirals that are LIRGs (under the assumption that merging systems are more affected by dust).

In this paper, we perform a quantitative study of the SFHs of a large sample of LIRGs in the nearby Universe ($z < 0.2$), by combining their UV (GALEX) and optical (SDSS; Adelman-McCarthy et al. 2004) photometry. This work utilises many of the theoretical tools that have been developed and successfully applied to GALEX-SDSS data from various galaxy populations, in particular early-types and E+A systems. The novelty of this study is (a) its quantitative nature - we quantify the SFHs of an unprecedentedly large sample of nearby LIRGs (b) the incorporation of the UV into the parameter estimation, which provides robust constraints on the recent SFH and (c) that we explore the role of AGN in these types of objects and search for signatures of feedback from the AGN on the SFH and gas content of their host galaxies.

In Section 2, we present the sample of galaxies used in this study and describe the process of visual inspection used to classify galaxies according to their morphology and interaction status. Section 3 describes the theoretical machinery used to quantify the SFH of each LIRG object in our sample. In Section 4 we explore the SFHs
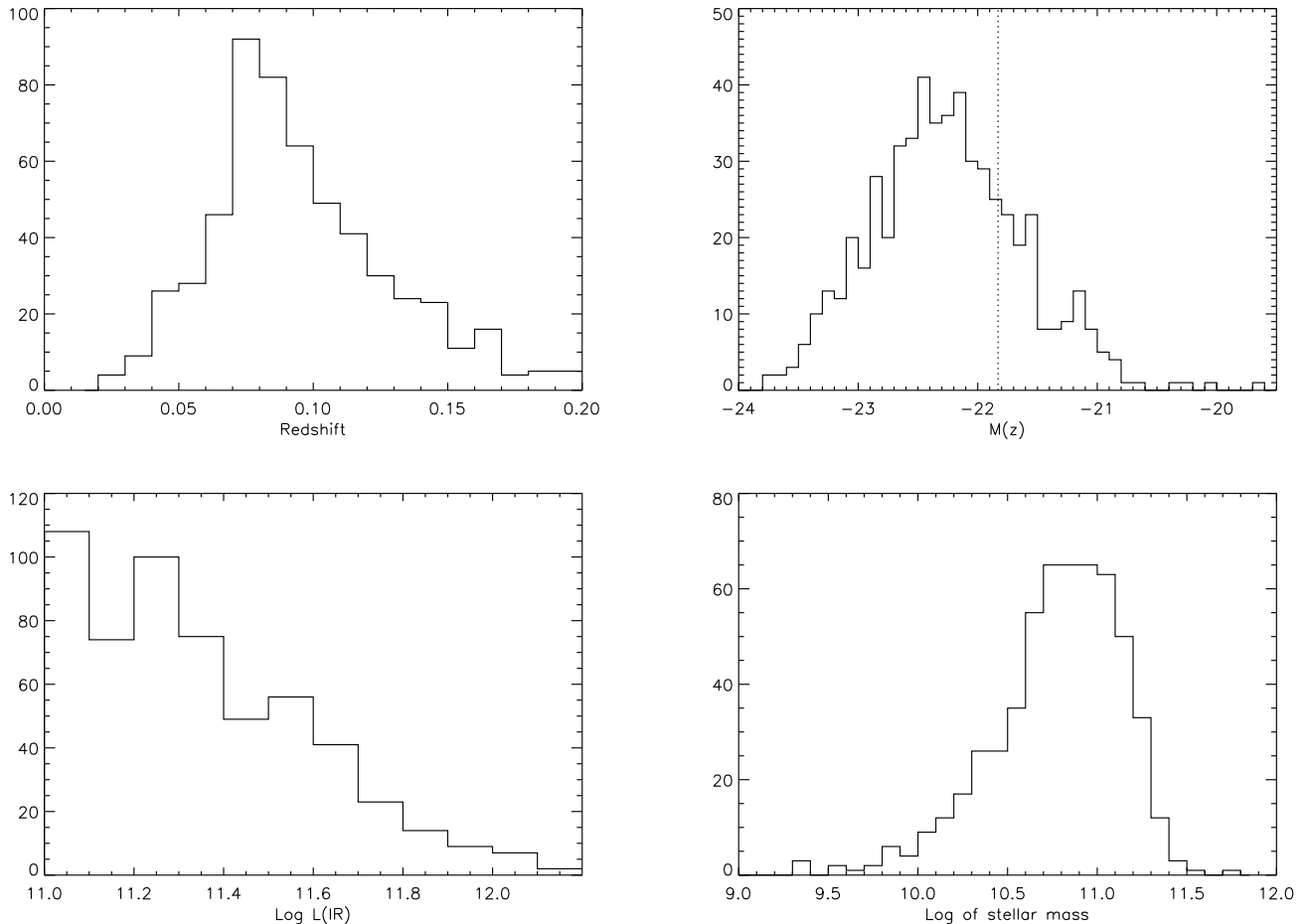
Figure 1. Basic properties of the LIRG sample studied in this paper. TOP LEFT: Redshift distribution from the SDSS. TOP RIGHT: Absolute z-band magnitudes. The value of M(z)* for early-type galaxies (Bernardi et al. 2003) is indicated by the dotted red line. Note that the *z*-band magnitudes are not K-corrected. BOTTOM LEFT: Far-infrared luminosities from Cao et al. (2006) in solar units. BOTTOM RIGHT: Stellar masses from Kauffmann et al. (2003b) in solar units.

of the LIRG population as a function of both their morphologies (early/late/mergers) and their interaction status (isolated/interacting/post-mergers), while in Section 5 we study the onset of AGN in these systems and explore whether there is plausible evidence for AGN feedback in these galaxies. Finally, in Section 6 we use the derived SFH parameters of spheroidal objects identified in this sample to explore the characteristics of major mergers in the nearby Universe.

2 THE SAMPLE

2.1 Photometric data and basic properties

Our study is based on a catalog of LIRGs, drawn from the SDSS Data Release 2 (DR2), compiled by Cao et al. (2006) by cross-correlating the IRAS Faint Source Catalog (Moshir et al. 1992) with the SDSS DR2. This catalog has been cross-matched with publicly available *UV* photometry from the third data release of the GALEX mission in its Medium Imaging Survey (MIS) mode (exposure time $\sim$ 1ks). We restrict ourselves to objects below a red-

shift of 0.2, since outside this range the GALEX filters do not trace the rest-frame UV. GALEX provides two *UV* filters: the far-ultraviolet (*FUV*), centred at $\sim 1530\AA$ and the near-ultraviolet (*NUV*), centred at $\sim 2310\AA$. This cross-matching produces 561 LIRGs with *at least* an MIS detection in the *NUV* filter, of which 413 have detections in both the *FUV* and the *NUV*. Note that we have removed Type I AGN from the sample because they could potentially contaminate the UV spectrum and skew our parameter estimation.

The final sample studied in this paper corresponds to the following limits: $0.02 < z < 0.2$, $m_r < 17.77$, $16.23 < m_{NUV} < 22.87$, $15.86 < m_{FUV} < 23.2$. The spectroscopic confidence (z_{conf}) is required to be better than 0.7 for each object. The redshift and magnitude limits of this study are similar to those of Wyder et al. (2007), who have performed a comprehensive analysis of the UV-optical colours of galaxies that have been detected in both the SDSS and GALEX surveys. Note however that, unlike this study, Wyder et al. (2007) also imposed a bright *r*-band cut of 14.5 mags, because the incompleteness of the SDSS spectroscopic coverage increases beyond this limit due to incomplete deblending of
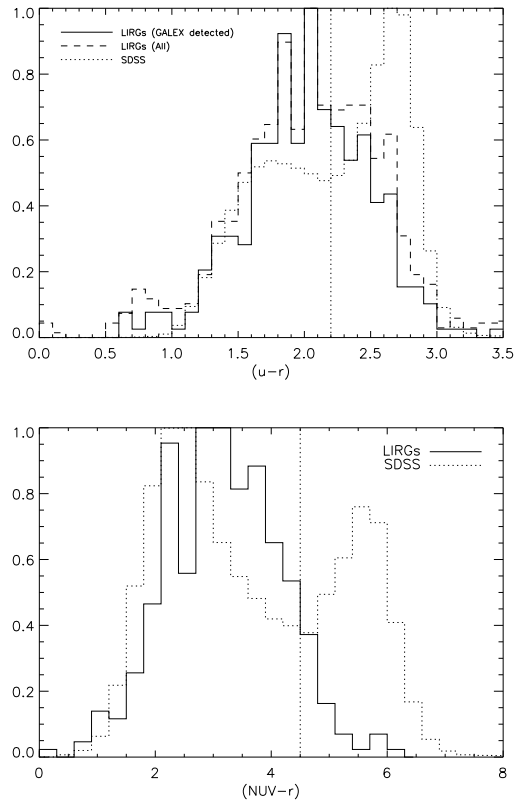
Figure 2. Comparison of the $(u-r)$ (top) and $(NUV-r)$ (bottom) colours of the LIRG population (solid lines) to the general galaxy population drawn from the SDSS (dotted lines). In both plots the separation between the blue and red peaks is indicated using a vertical dotted line. The comparisons are restricted to a volume limited sample ($z < 0.1$, $r < 17.77$). Note that while the relative proportions of galaxies in the red and blue peaks change depending on the magnitude cut employed, the colour at which the population divides remains stable (see e.g. Figure 2 in Strateva et al. 2001). For the $(u-r)$ comparison, we show histograms for both the LIRG population that has been detected by GALEX (solid line) and the full LIRG sample drawn from the SDSS (dashed line).

extended objects (see e.g. Strauss et al. 2002). We choose not to impose this cut here as only 1.3% of the sample studied in this paper has $r < 14.5$ and visual inspection of each object confirms that there are no anomalies in the SDSS pipeline processing.

In Figure 1 we present some basic properties of the LIRG sample used in this study - the redshift distribution, absolute z-band magnitudes, FIR luminosities and stellar masses. In Figure 2 we compare the $(u-r)$ and $(NUV-r)$ colours of the LIRG population (solid and dashed lines) to the general galaxy population drawn from the SDSS (dotted lines). Note that we show $(u-r)$ histograms for both the LIRG population that has been detected by GALEX (solid line) and the full LIRG sample drawn from the SDSS (dashed line). In both plots the separation between the blue and red peaks in the general galaxy population is indicated using a vertical dotted line. The comparisons are restricted to a volume limited sample in the SDSS at $z = 0.1$. While the relative proportions of general galaxies in the red and

blue peaks may change depending on the magnitude cut employed, the colour at which the population divides remains stable (see e.g. Figure 2 in Strateva et al. 2001).

We find that, in the $(u-r)$ colour, the LIRG population peaks around the colour bimodality point ($u-r \sim 2.2$) with a large fraction of the LIRGs falling in the blue cloud. In this optical colour the LIRG population seems to largely occupy intermediate colours between the blue cloud and red sequence. The situation in the $(NUV-r)$ colour is somewhat different. The LIRGs peak in the UV blue cloud, with a minor tail into the red sequence. The plots shown here are a useful benchmark for similar comparisons at high redshift. Both dust obscuration and the strength of star formation activity is likely to evolve with increasing look-back time and similar plots from high-redshift surveys are keenly anticipated.

Finally, we note some points regarding the SDSS and GALEX data that underpin this study. A potential concern for objects, typically for galaxies at low redshift, is pipeline 'shredding' of extended objects into smaller sub-components. In the very local Universe (redshifts lower than z=0.01), especially in large galaxies that have extremely irregular light distributions, shredding is a potential concern, particularly for GALEX detections in the shallowest All-sky Imaging Survey (AIS) mode (exposure time $\sim$100s) because the data is more noisy (Wyder et al. 2007, Ted Wyder, Mark Seibert priv comm.). For galaxies detected in the GALEX MIS mode, such as those used in this study, shredding is not an issue in our target redshift range ($0.02 < z < 0.2$). To ensure the quality of the GALEX data and the cross-matching to SDSS, a random 30% of the GALEX images were visually inspected to verify that (a) there was no evidence for shredding and (b) that cross-matching to the corresponding SDSS objects was robust. In addition, as a final check against deblending issues, we have checked that there is no systematic evolution in the average value or scatter of the $(NUV-r)$ colours of the LIRGs population, which would be expected if there was systematically higher shredding at lower redshifts.

Note that since each galaxy in this study is assigned a morphology and interaction status through visual inspection of its SDSS image (see next section), we can robustly verify a lack of shredding in the entire SDSS dataset used here. Finally, a minor fraction of GALEX objects ($\sim$ 20%, see e.g. Seibert et al. 2005) have multiple SDSS matches, due to detections in more than one GALEX field. For such objects, we select the GALEX detection with the highest exposure time for the subsequent analysis.

2.2 Visual inspection

A basic aim of this work is to correlate the SFHs of the LIRG population with their morphologies and 'interaction status'. We divide galaxies into three morphologies: 'early-types' (spheroidal or near-spheroidal objects that are likely to be the progenitors of elliptical galaxies), 'late-types' and 'mergers' (where *two* separate objects are involved and are already partially fused). The interaction status assigned to each object also falls into one of three categories: 'isolated', 'interacting/merging' or 'post-merger'. Systems that are morphologically identified as 'mergers' are automatically labelled as being 'interacting/merging'.
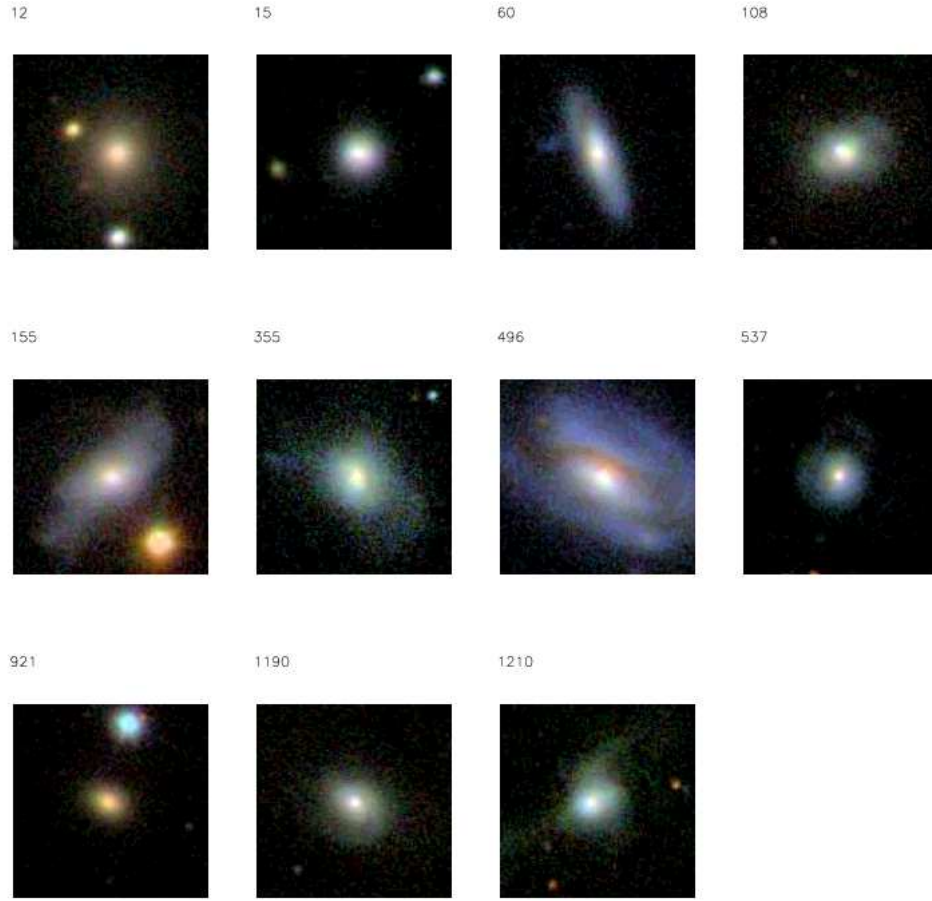
Figure 3. 'Early-type' galaxies identified in the LIRG population through visual inspection of the subsample of LIRGs that satisfy $r < 16.8$ and $z < 0.1$ (see Section 2.2 for the definition of early-type used in this study). Note that these objects typically show near-spheroidal morphology in their cores but exhibit morphological disturbances consistent with recent merging (108, 155, 355, 496, 537, 1190 and 1210). Object 496 is plausibly an 'NGC 5128 in the making'. Galaxy 60 appears to be in the final stages of accreting a small companion. While this object could be an inclined disk rather than a spheroid, it is most likely to be an S0 system with a dust feature in the northern part of the galaxy. The dust features appears to be spatially coincident with the accreted companion. Only three objects in this subset (12, 15 and 921) appear relaxed.

		Morphology			
		Early-types	Late-types	Mergers	
Interaction	No interaction	1.80%	61.15%		62.95%
	Int/merging	0.00%	13.67%	4.32%	17.99%
	Post-merger	2.16%	16.91%		19.07%
		3.96%	91.73%	4.32%	

Table 1. The LIRG sample split by morphology and interaction status (see Section 2 for descriptions of the categories). The totals for each category are shown in blue on the right and bottom ends of the table. Note that ongoing mergers are automatically labelled as interacting/merging. The sample is restricted to $r < 16.8$ and $z < 0.1$ since eyeball inspection from SDSS images is reliable within these magnitude and redshift ranges (see Section 2 in Kaviraj et al. 2007b).
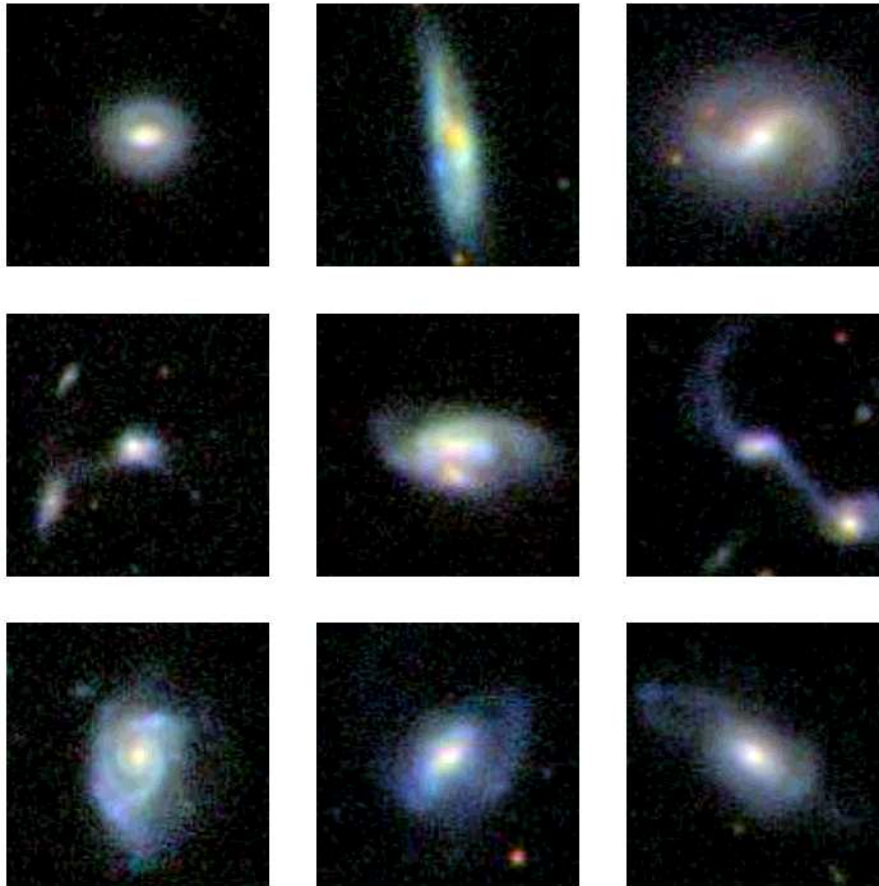
Figure 4. Examples of 'late-type' galaxies in the LIRG sample. The top row shows late-types classified as 'isolated'. The middle row shows late-types identified as 'interacting/merging', while the bottom row indicates late-types that are classified as 'post-mergers'.

While it becomes more difficult to decipher spiral features in higher redshift images, prior experience with early-type galaxies suggests that galaxy morphologies can be determined from SDSS images with good precision out to $z \sim 0.1$ if the objects have $r \lesssim 16.8$ (see Section 2 in Kaviraj et al. 2007b). In particular, if morphological classifications are kept fairly coarse (e.g. early/late), as is the case in this study, then tell-tale signs of disks can be successfully identified in the *composite* images, since disk-like features readily appear in the bluer optical filters (e.g. g-band).

We therefore begin by visually classifying all the objects in this sample that satisfy the fiducial criteria of $z < 0.1$ and $r < 16.8$. We present the results of this visual inspection in Table 1. We note first that, in agreement with previous studies of the LIRG population, the fraction of early-types is almost negligible. In Figure 3 we present *all* galaxies labelled as early-type in this visual inspection. Recall, however, that our definition of 'early-type' includes *near-spheroidal* objects which are likely to be progenitors of elliptical galaxies. It is apparent that many of galaxies in Figure 3, while having spheroidal cores, are not completely relaxed. Tidal features and evidence of accretion are widespread in the galaxy images indicating that they are merger remnants, although a few systems do exist that have relaxed morphologies, similar to the star-forming ellipticals discovered by Fukugita et al. (2004). Relaxed early-types with high LIRG-like SFRs are

likely to be very rare in the general galaxy population and their detection clearly depends on having a large sample of objects, as is the case in this study.

Since the early-type fraction is small, we are effectively left with two morphologies: mergers and late-types. In essence, this reduces to simply identifying the mergers, since the absence of early-types implies that all 'non-mergers' are late-types. Fortunately, given their distinct morphologies (typically double cores with asymmetric tidal distortions), mergers can readily be identified even when they are fainter than $r \sim 16.8$ or further away than $z \sim 0.1$. Since it is reasonable to assume that the fraction of early-types remains small across the entire redshift range of this study ($z < 0.2$), this also implies that we can extract a reasonably robust morphological classification, even in the subsample of galaxies that is fainter than $r \sim 16.8$ and further away than $z \sim 0.1$. We stress, however, that this *only* works for this particular sample because (a) our classification criteria are sufficiently coarse (early/late/mergers) (b) the early-type fraction is very small and (c) mergers can be readily identified even if the systems are relatively faint or distant. We also note that the interaction status of a galaxy can be determined accurately, even if the morphology of the object is uncertain. Identification of interacting/merging galaxies is straightforward, given the presence of an interacting neighbour and tidal bridges (which are readily visible in SDSS
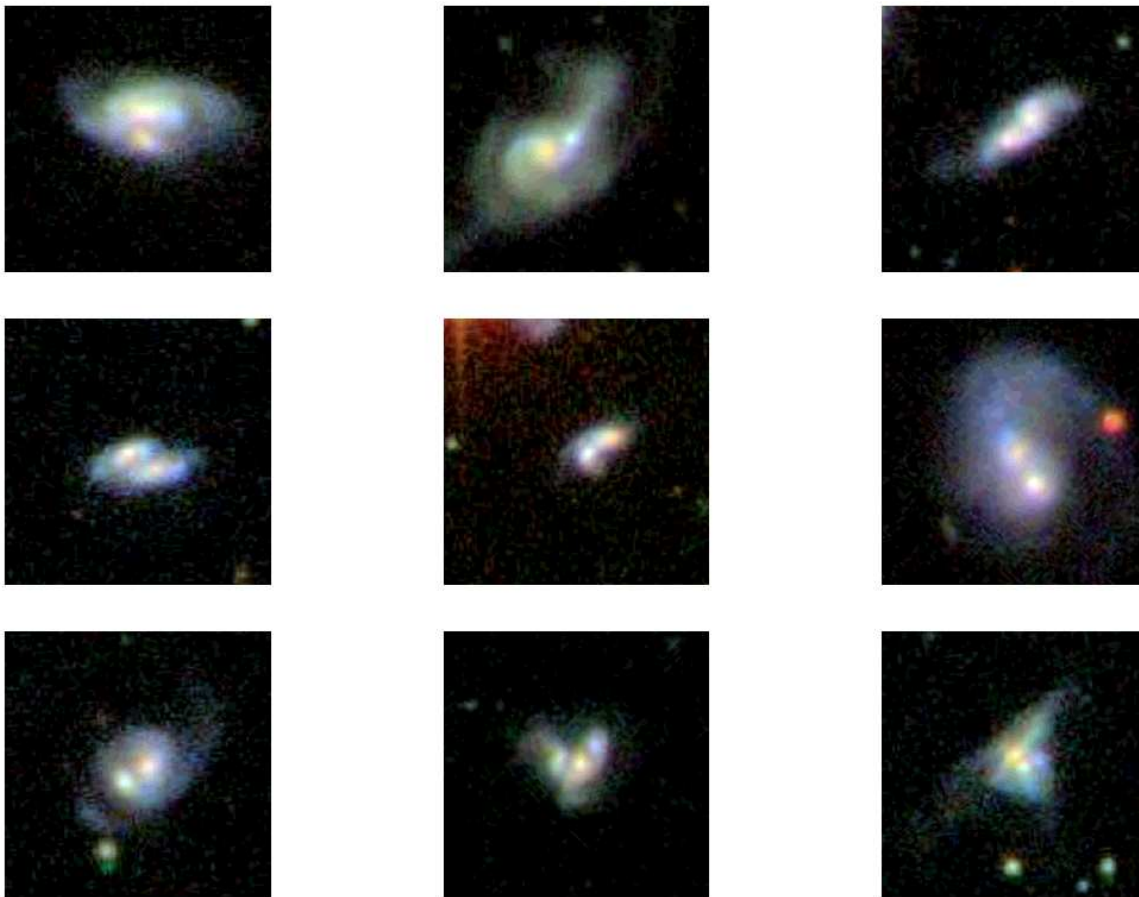
Figure 5. Examples of systems labelled as 'mergers' in the LIRG sample.

images of the nearby Universe). Post-mergers, i.e. systems where a single dominant central object shows asymmetric tidal features, are also readily identified.

Based on these arguments we visually classify all galaxies in terms their morphologies (early/late/mergers) and interaction status (isolated/interacting/post-mergers) in the redshift range $z < 0.15$. The redshift limit is chosen because (a) it encloses most of the galaxies in the sample (see Figure 1) and (b) because tidal distortions in post-mergers at the limit of this redshift range already appear quite faint and it might be difficult to detect such post-merger signatures in galaxies much further away. Note that we *only* attempt to identify early-types in the subsample of galaxies where $r < 16.8$ and $z < 0.1$. Therefore, the morphological classification for the complete sample of galaxies, where $z < 0.15$, is likely to be incorrect by $\sim 4\%$ (the early-type fraction found for $r < 16.8$ and $z < 0.1$). However, given that this is very small, it does not affect our subsequent analysis very significantly. Figure 4 shows examples of objects labelled as late-type. The top row indicates late-types classified as 'isolated'. The middle row shows late-types identified as 'interacting/merging', while the bottom row shows late-types that are 'post-mergers'. Finally, in Figure 5 we present examples of objects labelled as mergers.

We note that the visual classifications performed in this study are clearly limited by the depth of the SDSS images, which involve 50s exposures on a 2.5m telescope.

However, the detection of faint or red features may require deeper imaging. This is demonstrated by the recent work of van Dokkum (2005) who found widespread (and perhaps unexpected) post-merger signatures in a large fraction ($> 70\%$) of red early-type galaxies using $\sim$27,000 second exposures on 4m class telescopes. These tidal features extend to spatial scales > 50 kpc and are, almost without exception, undetectable in their shallower SDSS images. It is possible, therefore, that an unknown fraction of the LIRGs labelled as 'isolated' in this study may actually be post-mergers with very faint tidal features. While the tidal features in LIRGs are likely not to be red, indicating that this problem may not be as acute as for the red early-types in the van Dokkum (2005) study, it is likely that the fraction of LIRGs classified as isolated has been overestimated coupled with a corresponding underestimate of the LIRG population that are classified as post-mergers.

2.3 Stellar masses and AGN diagnostics

In addition to the photometric and visual inspection data, we use the publicly available Garching SDSS catalog[1] to add stellar masses and AGN diagnostics for each galaxy in our catalog. Type 2 AGN can be identified using combinations

---

[1] http://www.mpa-garching.mpg.de/SDSS/DR4/

of optical emission line ratios (see e.g. Baldwin et al. 1981; Kauffmann et al. 2003a; Brinchmann et al. 2004). Here, we use AGN classifications derived by Brinchmann et al. (2004) from line index measurements calculated using the code of Tremonti et al. (2004). Galaxies fall into one of three categories: AGN, composites (which show signatures of both AGN and star formation) and normal (where the emission lines are dominated by star formation or where the galaxy does not have the requisite S/N in the emission lines to perform a classification in the first place). Note that Type 1 AGN are removed from this analysis since their UV spectra is likely to be dominated by the active nucleus which, in turn, will perturb the parameter estimation used to quantify the SFHs. The stellar masses are taken from the catalog of Kauffmann et al. (2003b).

3 PARAMETER ESTIMATION

We estimate parameters governing the star formation history (SFH) of each LIRG in this sample by comparing its $(FUV, NUV, u, g, r, i, z)$ photometry to a library of synthetic photometry which is constructed using a large collection of model SFHs as follows.

Each model SFH is constructed by modelling the underlying population of the galaxy by a 'primary burst' (PB) which is assumed to be instantaneous, and the recent period of star formation (which is what we are primarily interested in) using an exponential burst. We refer to this recent episode as the 'secondary burst'. In the notation used below, we denote the primary burst using the subscript '1' and the secondary burst by the index '2'.

Figure 6 shows a schematic representation of the model SFHs. The principal free parameters in this analysis are the age of the primary burst (t_1), and the age (t_2), mass fraction (f_2) and timescale (τ_2) of the secondary burst. t_1 is allowed to vary from 1 Gyrs to 12 Gyrs, while t_2 is allowed to vary from 0.05 Gyrs to 12 Gyrs in the rest-frame of the galaxy. f_2 varies between 0 and 1 and τ_2 is allowed to vary from 0.01 Gyrs to 9 Gyrs. Since there are only two bursts, $f_1 = 1 - f_2$.

Since it is modelled as being instantaneous, the PB age (t_1) reflects the (SSP-weighted) *average* age of the underlying stellar population in the galaxy. As our subsequent analysis indicates, the values of t_1 are typically higher than 5 Gyrs, so that the primary burst does not affect the UV colours of the galaxy (which are dominated by stars less than 2 Gyrs old - see Figure 7 of Kaviraj et al. 2007b).

To build the library of synthetic photometry, each model SFH is combined with a single metallicity in the range $0.1Z_\odot$ to $2.5Z_\odot$ and a value of dust extinction parametrised by E_{B-V} in the range 0 to 1. Photometric predictions for each model SFH are generated by combining it with the chosen metallicity and E_{B-V} values and convolving with the stellar models of Yi (2003) through the GALEX FUV, NUV and SDSS u, g, r, i, z filters. Note that we use the empirical dust prescriptions of Calzetti et al. (2000) to compute the dust-extinced SEDs. This procedure yields a synthetic library of ~ 1.8 million models.

Since our sample is comprised of objects across a range in redshift, equivalent libraries are constructed at redshift intervals of $\delta z = 0.01$. A fine redshift grid is essential in such a low redshift study because a small change in redshift
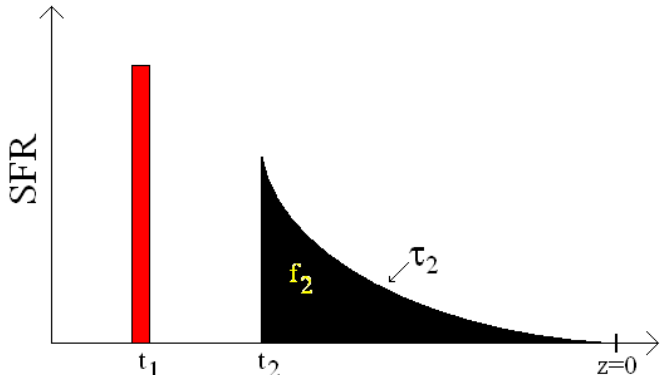

Figure 6. Schematic representation of model star formation histories (see Section 3 for details). t_1 is the primary burst (PB) age. t_2 is the secondary burst (SB) age. f_2 is the SB mass fraction and τ_2 is the SB timescale.

produces a relatively large change in look-back time over which the UV flux can change substantially, inducing 'K-correction-like' errors into the analysis.

Since the model library includes a large range of dust values and the UV colours are sensitive to dust, we wish to avoid including models in our parameter space where a spuriously large RSF fraction (i.e. f_2) may fit the UV colours of a galaxy due to an unreasonably high dust extinction. This is not just desirable but also necessary, since the results of Burgarella et al. (2005) imply that the nearby LIRG sample satisfies $A(FUV) \sim 2.7$ (which translates to $E_{B-V} \sim 0.3$ using a standard Calzetti dust law). Since the available values of E_{B-V} in the model library spans $0 < E_{B-V} < 1$, we apply a prior to the E_{B-V} parameter space to ensure realistic values of dust extinction are employed for each LIRG.

In the local Universe, the obscuration in star-forming galaxies correlates with the FIR luminosity (e.g. Calzetti et al. 1995; Wang & Heckman 1996; Adelberger & Steidel 2000; Hopkins et al. 2001). Following Hopkins et al. (2001, see their Eqns. 1, 2 and 3) we estimate the dust extinction in the nebular emission lines (E_{B-V}^G) for each galaxy from the FIR luminosity and convert it to a value appropriate for the stellar continuum E_{B-V}^S using $E_{B-V}^S = 0.44 \times E_{B-V}^G$ (Calzetti et al. 2000). The prior on the dust is applied, for each galaxy, by restricting the model library to $E_{B-V}^S \pm 0.1$. It is worth noting that the applied prior is not particularly strong. A large range of *realistic* dust values is permitted for each galaxy *but the E(B-V) parameter space typically greater* $E_{B-V}^S \sim 0.5$ *is discarded*.

Converting the values of E_{B-V}^S derived using the procedure described above to A_{FUV} using a Calzetti law yields $1.8 < A_{FUV} < 3.3$ for our sample of LIRGs. This compares very well with the recent LIRG study of Burgarella et al. (2005a) who find a median obscuration of $A_{FUV} = 2.7 \pm 0.8$, using theoretical calibrations derived from GALEX and IRAS data by Buat et al. (2005). Note that Buat et al.'s calculations are resistant to the choice of the exact extinction curve (see their Section 3.1).

The principal free parameters (t_1, t_2, f_2 and τ_2) are estimated by comparing each observed galaxy to every model in the synthetic library, with the likelihood of each model
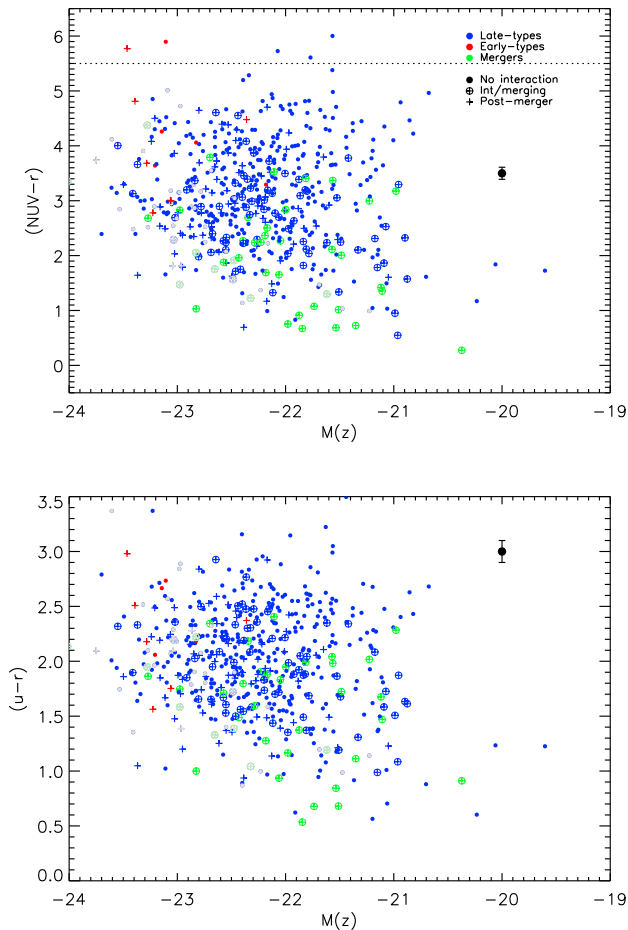
Figure 7. TOP: The $(NUV - r)$ colour-magnitude relation (CMR). The NUV filter is centred at $2300\text{\AA}$. BOTTOM: The optical $(u - r)$ CMR. Morphologies are shown colour-coded and symbol types correlate with the interaction status of the object (see Section 2.2 for details). The dotted line in the top panel indicates the position of the UV 'red sequence', taken from a study of the nearby early-type population (Kaviraj et al. 2007b). The morphological classifications were performed only for objects with $z < 0.15$ (see Section 2.2 for details). Galaxies outside this redshift range are shown in grey.

$(\exp - \chi^2/2)$ calculated using the value of χ^2 computed in the standard way. From the joint probability distribution, each parameter is marginalised to extract its one-dimensional probability density function (PDF). We take the median of this PDF as the best estimate of the parameter in question and the 16 and 84 percentile values as the uncertainties on this estimate.

For galaxies which do not have FUV detections, the parameter estimation is performed using only the NUV, u, g, r, i and z-band filters. We do not use the FUV detection limit as an upper limit to the FUV flux, primarily because the uncertainties on the estimated parameter effectively become unbounded. Previous work on early-type galaxies and E+A systems indicates that addition of the FUV filter does not affect the median values but does reduce the size of the uncertainties. The cosmological param-

eters used in this study assume a ΛCDM model: $h = 0.7$, $\Omega_m = 0.3$ and $\Omega_\Lambda = 0.7$.

4   STAR FORMATION HISTORIES

It is instructive to look first at the UV and optical colour-magnitude relations of the LIRG population, since the derived SFHs are effectively driven by the observed colours (Figure 7). Morphologies are shown colour-coded and symbol types correlate with the interaction status of the object. The dotted line in the top panel indicates the position of the UV 'red sequence', taken from a study of the nearby early-type population (Kaviraj et al. 2007b). Not unexpectedly, virtually all LIRGs lie away from the red sequence, notwithstanding their relatively high dust content. The bulk of the sample occupies the 'blue cloud' ($NUV - r < 3.5$). We note that the distributions in both the UV and optical colours are very broad and that smaller galaxies are not preferentially bluer as typically indicated by the downsizing phenomenon (see e.g. Cowie et al. 1996). However, the star formation regimes in these objects are significantly more severe than in the normal galaxy population and the observed colours are dominated by the vigorous RSF being experienced by these systems. Since the downsizing phenomenon reflects the make-up of the underlying stellar population of galaxies that forms over the lifetime of the Universe, it is reasonable to expect these trends to be temporarily washed out by the strong RSF in the LIRG sample.

We now present the derived SFHs for galaxies in the LIRG sample. We explore these SFHs, both as a function of the morphology of the galaxies, as well as their interaction status. In Figure 8 we begin by presenting the derived SFH parameters, split by the morphology of the galaxies. The top-left, top-right, bottom-left and bottom-right panels show the distributions of PB ages (t_1), SB ages (t_2), SB mass fractions (f_2) and SB timescales (τ_2) respectively.

The distribution of PB ages (t_1) peaks around ~ 7 Gyrs, with the bulk of the sample satisfying $5 < t_1 < 9$ Gyrs (the average value is ~ 6.8 Gyrs). Recall that the values of t_1 reflect the (SSP-weighted) *average* ages of the underlying stellar populations. Note that, since the UV is sensitive only to populations with ages < 2 Gyrs, the estimates of t_1 are driven primarily by the optical filters. Given their lower sensitivity to young stellar populations, the uncertainties in the values of t_1 are high (~ 1.2 Gyrs). Nevertheless, it is worth noting that very few of the galaxies have underlying populations that are well-fit by purely old (> 10 Gyrs) stellar populations. This result is not unexpected, since the LIRG sample is dominated by late-type galaxies, which have typically formed stars over the lifetime of the Universe.

The top-right panel of Figure 8 indicates that roughly 60% of the LIRGs in this study began their RSF episode within the last Gyr (i.e. SB age or $t_2 < 1$ Gyr), while for the remaining galaxies $1 < t_2 < 3$ Gyrs. Virtually none of the objects exhibit $t_2 \gtrsim 3$. The mergers (green) have a distribution in t_2 that is sharply peaked below $t_2 < 0.5$ Gyrs, consistent with the fact that their RSF episodes have begun recently or, at least, are still in progress. The bottom-left panel of Figure 8 indicates that nearby LIRGs have formed up to 35% of their stellar mass in the recent star formation episode. The mean value is $\sim 15\%$. Not unexpectedly, the
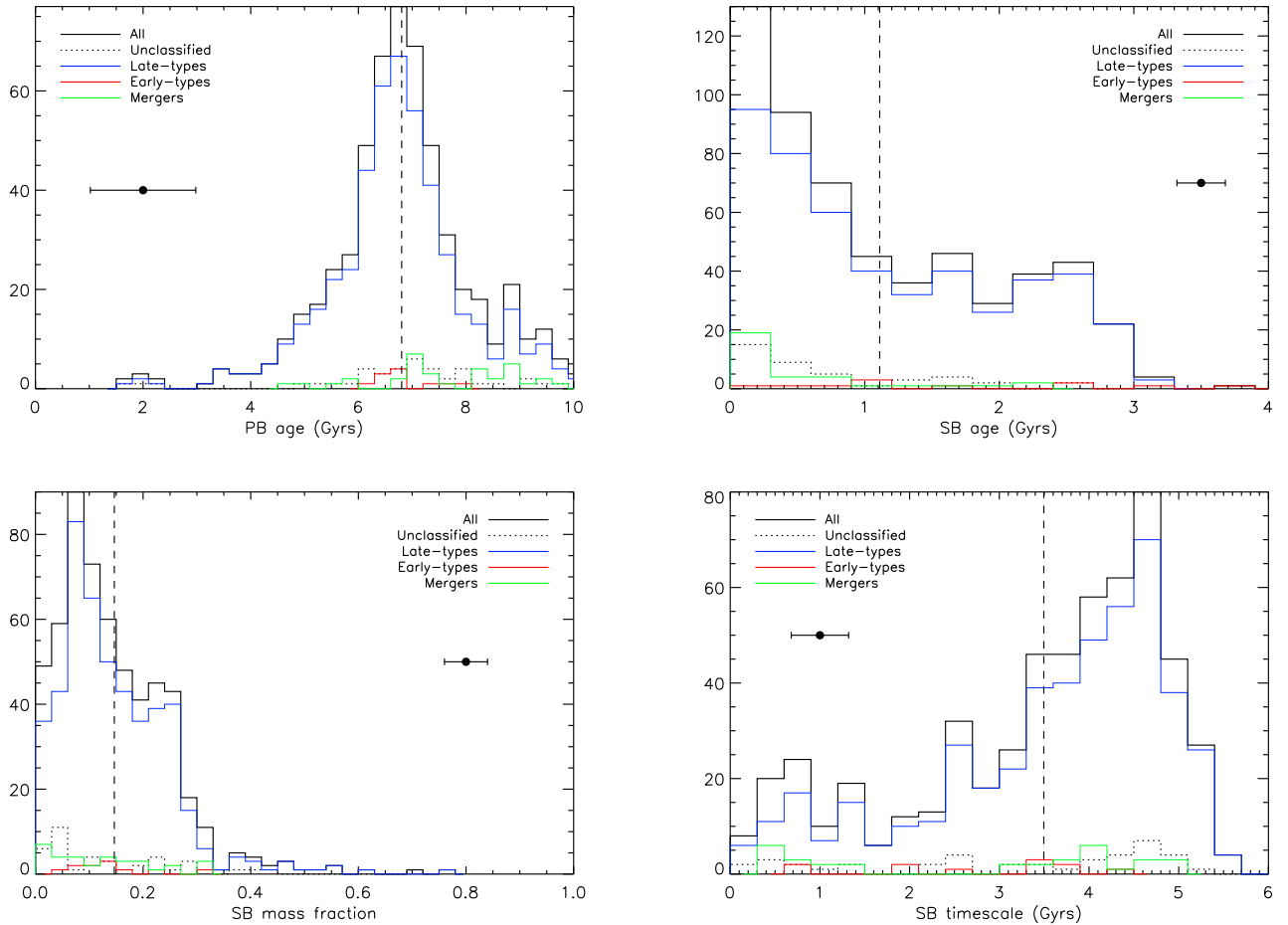
Figure 8. The derived SFHs of the LIRG sample as a function of the morphology of the galaxies. TOP-LEFT: The primary burst ages (t_1). TOP-RIGHT: The secondary burst ages (t_2). BOTTOM-LEFT: The secondary burst mass fractions (f_2). BOTTOM-RIGHT: The secondary burst timescales (τ_2). The mean value of each parameter for the population as whole is indicated by the vertical dashed lines. The morphological classifications were performed only for objects with $z < 0.15$ (see Section 2.2 for details). The 'unclassified' category contains all objects outside this redshift range.

mergers (green) peak towards lower mass fractions, since the SF episode is less advanced than in the other morphological types. The bottom-right panel of Figure 8 indicates that the SB timescales (τ_2) involved in these events are typically large, of the order of a few Gyrs, indicating that the SFR does not decline significantly during the course of the RSF episode.

In Figure 9, we briefly present the SB ages of the LIRG sample as a function of their interaction status. The PB ages (t_1), SB mass fractions (f_2) and SB timescales (τ_2) are omitted for clarity, as all categories (isolated/interacting/post-mergers) have similar distributions in these variables, akin to the ones presented in Figure 8. We find that around 74% of the galaxies that are currently interacting systems began their RSF episodes within the last 0.5 Gyrs. Recall that the 'interacting/merging' category includes all systems that are currently interacting, not just mergers which are a special case where two systems are partially fused.

Finally, in Figure 10, we summarise the SB ages and SB mass fractions of individual galaxies in our sample. Morphologies are shown colour-coded and symbol types indi-

cate the interaction status of each galaxy. Since the morphological classifications were performed only for objects with $z < 0.15$ (see Section 2.2), objects outside this redshift range are shown in grey.

5   THE ROLE OF AGN

Several lines of theoretical and observational evidence indicates that AGN, driven by supermassive black holes that inhabit galactic centres, are likely to play a significant role in the formation and evolution of their host galaxies. The principal impact of AGN is energetic feedback on the inter-stellar medium (ISM) which acts to remove (cold) gas from the potential well halting star formation in massive galaxies (e.g. Silk & Rees 1998; Benson et al. 2003; Silk 2005). Such negative feedback from AGN is commonly invoked in galaxy formation models to reproduce the cut-off in the galaxy luminosity function at high luminosities (Benson et al. 2003) and to fit the observed colours of massive galaxies at present-day (Kaviraj et al. 2005; De Lucia et al. 2006). Without such feedback, the potentially plentiful supply of cold gas in mas-
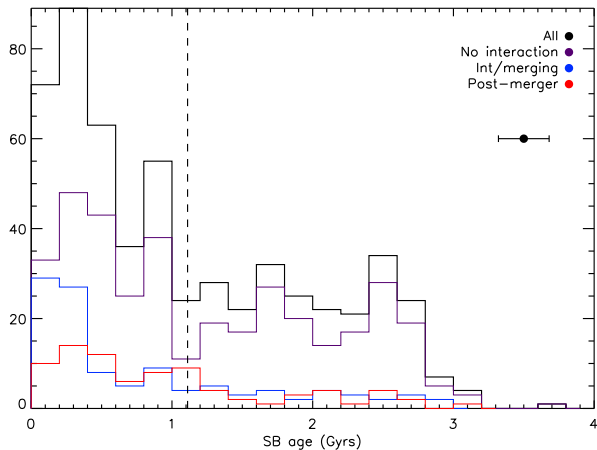
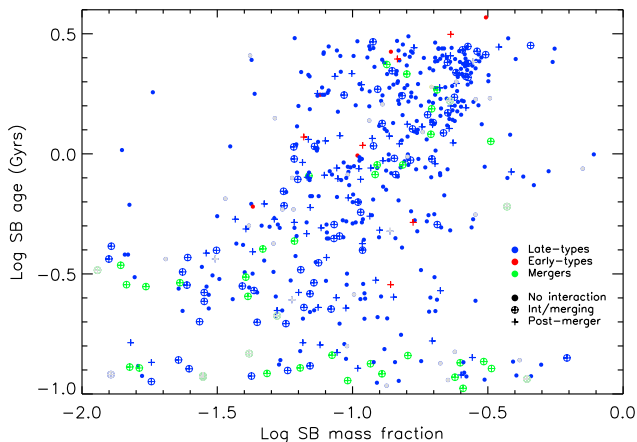**Figure 9.** The secondary burst ages (t_2) as a function of the interaction status of the LIRGs in our sample.

Figure 10. The secondary burst ages (t_2) and mass fractions (f_2) of our LIRG sample. The morphology of the galaxies is shown colour-coded and their interaction status is shown using different symbol types. Note that the morphological classifications were performed only for objects with $z < 0.15$ (see Section 2.2 for details). Objects outside this redshift range, which were not part of the morphological classification, are shown in grey.

sive galaxies results in objects that are predicted to be too massive and too blue to fit the observations in the nearby Universe. Since low-redshift LIRGs represent some of the most vigorously star forming galaxies in the nearby Universe, it is instructive to explore the potential role of AGN in these systems and search for tell-tale signs of feedback in their SFHs.

5.1 Number fractions and morphologies of AGN hosts

We begin by exploring the proportion of AGN in the LIRG sample studied in this paper. The overall fraction of AGN is $\sim 14\%$. We find that the AGN fraction shows a dependence on the interaction status of the galaxies - it rises from
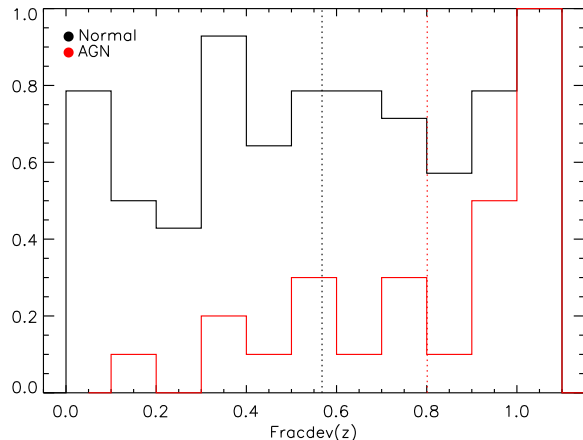

Figure 11. Comparison of the bulge/disk morphologies of LIRGs that host AGN (red), to those that show composite spectra (green) and those that do not show any indication of an AGN (black). Note that we restrict the sample to nearby ($0.06 < z < 0.09$) objects for this comparison, to ensure the accuracy of the light profiles and explore the `fracdev` parameter in the z-band filter which is least affected by the RSF and therefore traces the bulk stellar population of the galaxy most faithfully.

13.1% in non-interacting objects to 17.6% in the interacting population and back down to 13.4% in the post-mergers, strongly consistent with the idea that interactions trigger the onset of AGN. A similar result has been found recently by Alonso et al. (2007) in nearby close pairs drawn from the SDSS. Their results indicate that the AGN fraction in close pairs that exhibit definite signs of interactions is $\sim 4\%$ higher than in pairs that are not interacting. This value is strikingly similar to the corresponding statistics found in our LIRG sample. We should note, however, that the number of galaxies in the non-interacting and post-merger categories is fairly small (of the order of a 100 objects each). Thus, while the trend in the AGN fraction is qualitatively similar to previous works, the low number statistics make it difficult to ascertain how significant the change in the AGN fraction really is.

Previous studies of the AGN population have indicated that they typically reside in massive bulge-dominated systems (Kauffmann et al. 2003a). While our sample of LIRGs is a subset of the galaxy populations studied before, it is instructive to look at the distribution of bulge/disk morphologies of AGN in these galaxies, since they are far more extreme in terms of their star formation properties than the normal galaxy population. We compare the bulge/disk morphologies of the AGN hosts in this sample to galaxies without AGN using the SDSS `fracdev` parameter. The SDSS pipeline fits both a deVaucouleur's and an exponential model to the light profile of each galaxy in the u, g, r, i, z filters. A composite *best-fit* is then generated using a linear combination of the two fits. `fracdev` is the weight of the deVaucouleur's model in this composite fit and provides a quantitative measure of the bulge component of the galaxy. Early-type galaxies in the nearby Universe typically have `fracdev`> 0.85.

In Figure 11 we compare the `fracdev` distribution of

the AGN hosts to that in the normal galaxies. Note that we restrict the sample to nearby ($0.06 < z < 0.09$) objects to ensure the accuracy of the fitted light profiles and explore the `fracdev` parameter in the z-band filter which is least affected by the RSF and therefore traces the bulk stellar population of the galaxy most faithfully. We find that, consistent with previous results, the distribution of the AGN hosts is strongly skewed towards higher values of `fracdev`, while the normal galaxy population shows a flat distribution in this parameter. We conclude that AGN, even in the most strongly star-forming systems in the nearby Universe, occupy galaxies which have a dominant bulge component.

5.2 Colours and star formation histories of the AGN hosts

Given their significance in galaxy formation models, it is useful to constrain the role of AGN in the LIRG population studied here. We wish to explore (a) the time after the onset of star formation when the AGN typically appears and (b) whether there is any evidence of negative feedback from AGN in their host galaxies. Both these aims can be achieved by comparing the derived SFHs of the AGN hosts to that of the normal galaxies.

In Figure 12 we compare the colours of the AGN hosts (red), to those that show composite spectra (green) and galaxies that do not show any indication of an AGN (black). We find that, irrespective of the colour, the AGN hosts are consistently redder than the normal galaxies. The mean values (indicated using dotted lines) show that AGN are redder in $(NUV - r)$, $(u - r)$ and $(g - r)$ by ~ 1.2, ~ 0.6 and ~ 0.4 mags respectively. The systematic reddening persists if we split the sample into luminosity bins and/or explore different redshift ranges. The reddening in colour could be produced either by an enhanced dust content in AGN or by a systematic difference in their SFHs. Clearly both explanations have to be explored before the colour discrepancy can be explained.

We find that the distributions of E_{B-V} do not indicate a systematic dust enhancement in the AGN hosts [2] leading us to consider the alternative explanation for the reddening in the AGN colours - that they are driven by a systematic difference in their SFHs. In Figure 13 we compare the derived SFH parameters of the AGN, composites and normal galaxies. We find that the distributions of PB ages (top-left panel) are virtually identical for all categories, implying that the underlying populations of the galaxies are very similar. The SB timescales are also consistent between the three categories (bottom-right panel). The principal difference in the SFHs is that the SB ages of the AGN hosts show an offset of ~ 0.6 Gyrs compared to the normal galaxies. In particular,

[2] In fact, the discrepancies in the colours themselves do not favour a differential dust content as an explanation for the redder colours in the AGN hosts. While a small differential dust extinction can, in principle, produce a large offset in the UV colour (because e.g. $A_{(NUV-r)} \sim 6 \times E_{B-V}$), the extinction in the $(g - r)$ colour is $A_{(g-r)} \sim 1.09 \times E_{B-V}$ using the Calzetti dust law. If the SFHs of the AGN hosts and the normal galaxies were identical, it is difficult to explain the observed average discrepancy in $(g - r)$ (~ 0.4 mags), by simply invoking a systematic E_{B-V} offset of ~ 0.4 mags.
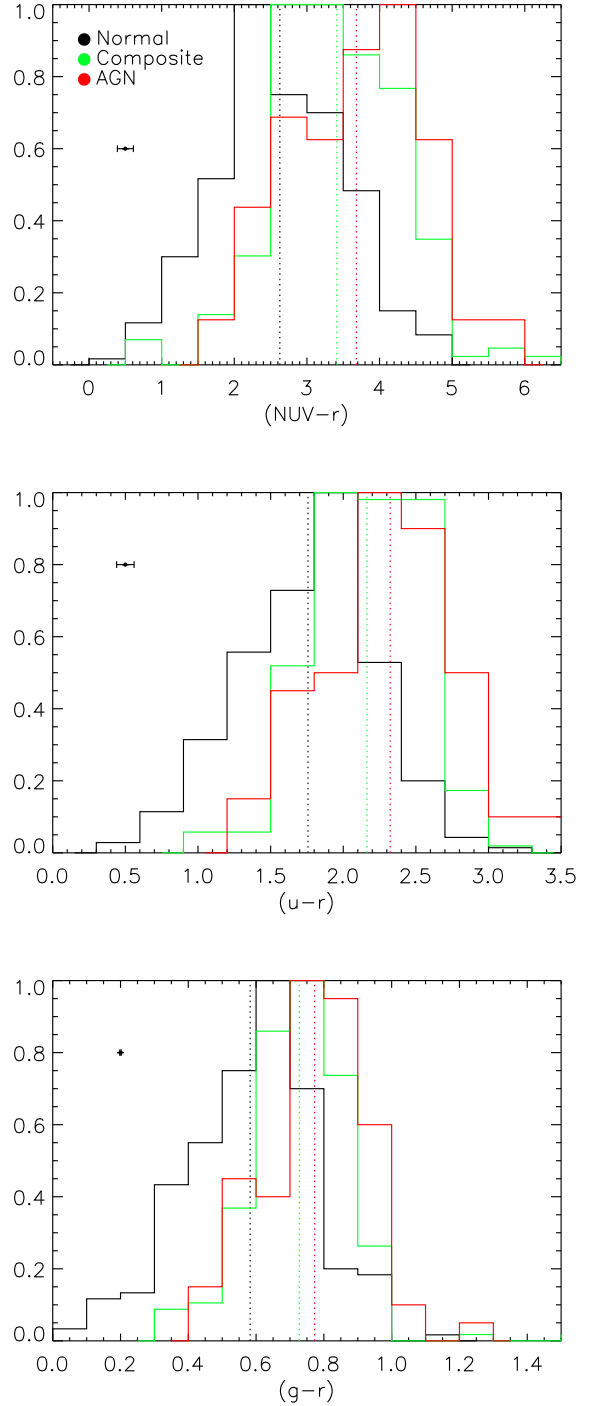

Figure 12. Comparison of the colours of LIRGs that host AGN (red), to those that show composite spectra (green) and those that do not show any indication of an AGN (black).

the distribution of SB ages in the AGN declines dramatically at values less than $\sim 0.5 - 0.7$ Gyrs.

These results indicate that the SFHs in AGN do not differ significantly from those in the normal galaxies but that we are simply observing the AGN hosts a *longer* time after the onset of star formation (since the SB ages are larger).
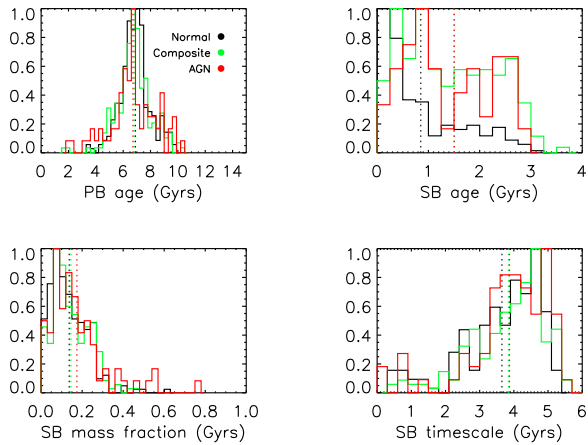
Figure 13. Comparison of the SFHs of AGN, composites and normal galaxies in the LIRG sample. Note that the histograms for all populations have been normalised to 1. The fraction of AGN in the LIRG sample studied here is $\sim 14\%$.

The rapid decline in the number of AGN at SB ages less than $\sim 0.5 - 0.7$ Gyrs suggests that AGN typically appear $\sim 0.5 - 0.7$ Gyrs after the onset of star formation. It is worth noting that a similar time delay (a few hundred Myrs) between the peak of the star formation and the rise of the AGN has been reported in a recent study of AGN activity in early-type galaxies (Schawinski et al. 2007).

The similarity between the properties of the star formation in the AGN hosts and the normal galaxies indicates that the AGN itself does not have a measurable impact on the SFHs of their host galaxies. Negative feedback can be expected to remove or heat cold gas from the potential well, leading to a reduction in the star formation activity. If star formation is strongly quenched, we would expect the decay timescale of the star formation activity to decrease, as the SFR is strongly reduced by removal of cold gas from the system. This, in turn, will be reflected in a reduction of the SB timescales. Such an effect on the SB timescales is clearly seen in post-starburst (E+A) galaxies, where the lack of Hα in emission, coupled with deep Balmer lines, indicates that a vigorous period of star formation has been rapidly quenched (Kaviraj et al. 2007c). However, as Figure 13 indicates, we find no evidence for a similar effect in the LIRG population. In fact the average SB timescales (see the vertical dotted lines) in the AGN hosts are marginally larger.

As a further check of this result, we compare the evolution of the cold gas fractions in the AGN hosts to that in the normal galaxies (Figure 14). Following Wang et al. (2006) we estimate the cold gas mass using the correlation between the CO and IR luminosities derived by Gao & Solomon (2004a, by combining their Eqns 1 and 2), and apply the 'standard' CO-to-H$_2$ ratio estimated from giant molecular clouds in the disk of the Milky Way (see Eqn. 5 in Gao & Solomon 2004b). Note that, since there is an evolution in the gas fraction as a function of mass/luminosity in the LIRG population (see Figure 5 in Wang et al. 2006), we split Figure 14 into three luminosity bins in $M(z)$ with roughly equal numbers of objects.

If the AGN are depleting the cold gas reservoirs in their

host galaxies then we would expect to see - *at a given value of SB age* - a systematically lower cold gas content in the AGN hosts than in the normal galaxies. Figure 14 indicates that, as should be expected, the cold gas fractions show a steady decline with SB age, regardless of the luminosity bin being considered. However, it is also apparent that the AGN do not show a preferentially lower cold gas content and that the trends in the AGN are indistinguishable from those in the normal galaxies. The lack of discrepancy in the cold gas content *independently* supports the observed similarity in the SFHs of the AGN and their normal counterparts. We conclude, therefore, that there is no measurable evidence for feedback in LIRGs that host Type 2 AGN, either in terms of cold gas removal or the impact on the SFH that would result from such gas depletion.

6 LIRGS WITH SPHEROIDAL MORPHOLOGIES - MIXED MAJOR MERGERS?

The sample of spheroidal objects identified in this study (Figure 3) allows us to explore the star formation that is plausibly induced by (gas-rich) major mergers in the nearby Universe. In this section we summarise the characteristics of such major merger driven star formation and speculate on the properties of the progenitors involved, using the derived SFH parameters of these spheroidal galaxies.

We note first that the early-type galaxies identified in the visual inspection (shown in red in Figure 8) have PB ages (t_1) of ~ 6.9 Gyrs. Based on the fact that (a) these objects have spheroidal morphology (b) exhibit LIRG-like SFRs and (c) contain underlying populations with relatively young average ages, we speculate that they are the products of 'mixed' major mergers where *at least* one of the progenitors has late-type morphology. This is because mergers between two ellipticals should result in higher values of t_1, since the red optical colours of the elliptical population would require both galaxies to have stellar populations that are overwhelmingly old (> 10 Gyrs old). Furthermore, since ellipticals are typically gas-poor systems, a dry major merger (or equally a minor merger, see e.g. Figure 1 in Kaviraj et al. 2007d) would not supply enough gas to create the high LIRG-like SFRs in these systems.

In Figure 15 we summarise the SFHs of the early-type objects in this sample. The points are colour-coded using the $(NUV - r)$ colour, symbol sizes correlate with the SB timescales and galaxy images are placed next to the data points to demonstrate their morphologies. We find that such 'mixed' major mergers, that produce LIRG-like objects in the local Universe, typically form between 5 and 30% of the stellar mass in their remnants. The duration of these events is between 0.3 and 4 Gyrs, although, since most of the objects are unrelaxed, these values are typically lower limits. The star formation timescales range between 0.7 and 4.2 Gyrs and comparison of the SB ages and SB timescales in Figure 15 indicates that the SFR does not decline significantly through the event.
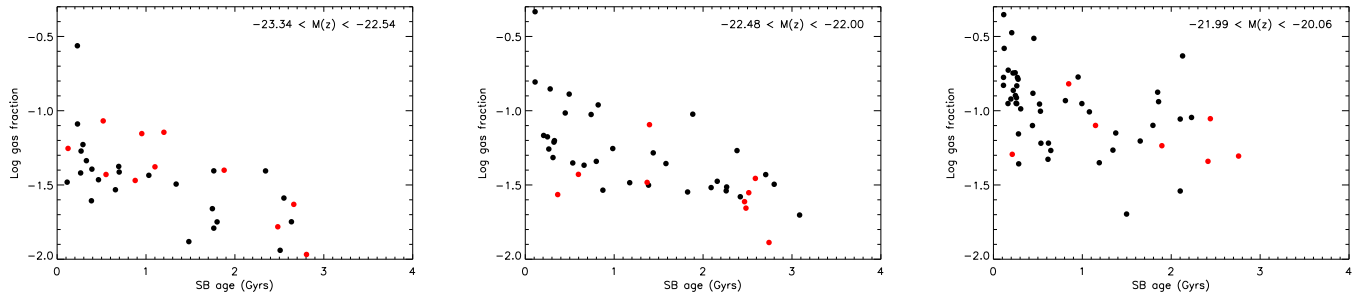
Figure 14. The evolution of the cold gas fraction as a function of the age of the secondary burst (i.e. the SB age parameter) in the AGN hosts (red) and normal galaxies. Note that, since the cold gas fraction decreases with the luminosity of the galaxy (see Figure 5 in Wang et al. 2006), we bin the sample into three luminosity bins in $M(z)$ with roughly equal numbers of objects and consider a narrow redshift range ($0.06 < z < 0.09$).

7   SUMMARY AND CONCLUSIONS

We have performed a quantitative study of the SFHs of 561 LIRGs in the low-redshift ($z < 0.2$) Universe. The sample consists of galaxies in the SDSS DR2 that satisfy the LIRG criterion ($L_{IR} > 10^{11} L_\odot$) in their IRAS fluxes and are detected by the GALEX UV space telescope.

A visual inspection of a subsample of galaxies with $r < 16.8$ and $z < 0.1$ (for which eyeball classification of galaxy morphologies is reliable) indicates that the fraction of spheroidal or near-spheroidal objects that could be progenitors of elliptical galaxies, is small (4%). The remaining objects are morphologically late-type or ongoing mergers. 61% of the population do not show any indication of interactions at the fiducial depth of the SDSS images, while the remaining objects are either in the process of interacting (18%) or show post-merger morphologies (19%).

Notwithstanding their high dust content ($< E_{B-V} > \sim$ 0.3), the overwhelming majority of low-redshift LIRGs lie in the UV blue cloud. We have parametrised the SFH of each galaxy in our sample by comparing their GALEX (UV) and SDSS (optical) photometry to synthetic photometry from a large library of ~ 1.8 million model SFHs. We find that the (SSP-weighted) *average* age of the underlying stellar populations in these objects is typically between 5 and 9 Gyrs, with a mean value of ~ 6.8 Gyrs. Roughly 60% the LIRG population began their recent star formation (RSF) episode within the last Gyr, while the remaining objects are consistent with values between 1 and 3 Gyrs in the past. The age of this recent burst does not exceed ~ 3 Gyrs in virtually any of the objects in this sample. LIRGs in the low redshift Universe have formed up to 35% of their stellar mass in this recent episode - the mean value is 15%. The star formation timescales are large ($\sim$a few Gyrs), indicating that the SFR does not decline significantly during the course of the burst.

14% of the LIRG population host a Type 2 AGN. The AGN fraction rises from 13.1% for non-interacting objects to 17.6% for the interacting population and back down to 13.4% for the post-mergers, possibly supporting the hypothesis that interactions trigger the onset of AGN. However, the numbers of objects in each category are small and, while a trend does exist, the low number statistics make it difficult to establish a robust result.

In agreement with previous studies, the distribution of bulge/disk morphologies (derived from the SDSS `fracdev`
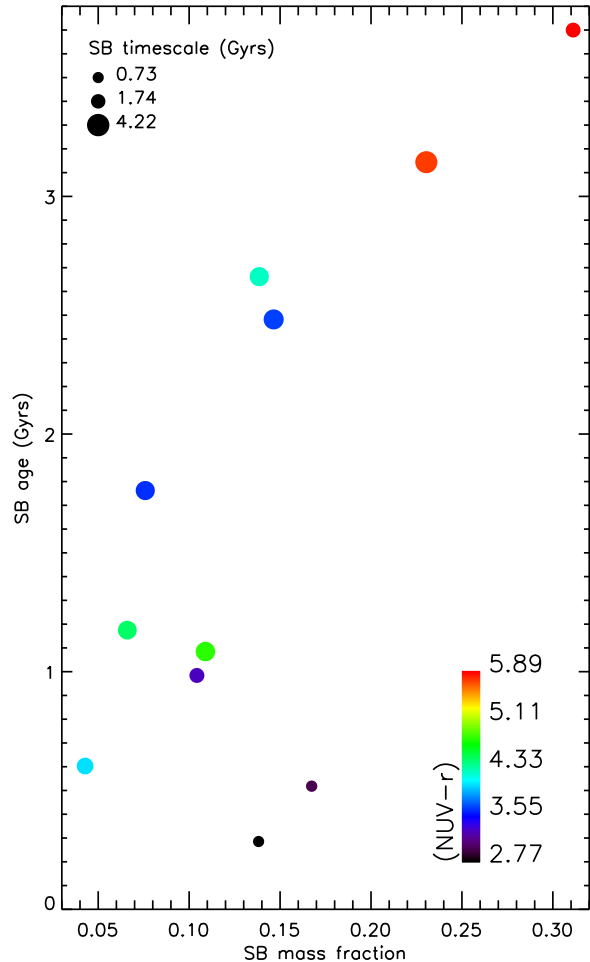

Figure 15. The derived SFH parameters of spheroidal objects in the LIRG sample. See Figure 3 for a description of the sample.

parameter) in the AGN hosts favours systems which have a significant bulge component (`fracdev`$\gtrsim 0.6$), in contrast to the normal LIRGs which have a flat distribution in `fracdev`.

Comparison of the UV and optical colours of the AGN hosts to those of the normal galaxies indicates that the AGN

are consistently redder than the normal population in both the UV and the optical colours. We find that the AGN are redder in $(NUV - r)$, $(u - r)$ and $(g - r)$ by ~ 1.2, ~ 0.6 and ~ 0.4 mags respectively. The systematic colour offsets persist even if we split the sample into luminosity bins and/or explore different redshift ranges. The distributions of E_{B-V} values do not indicate a systematic dust enhancement in the AGN hosts. Comparison of the derived SFH parameters indicates that, while the underlying populations and e-folding timescales of the star formation in AGN do not differ from those in the normal galaxies, the ages of the RSF episodes in the AGN are older (producing the redder colours), indicating that we are simply observing the AGN hosts a *longer* time after the onset of star formation. The derived SFH parameters indicate that the AGN typically appear $\sim 0.5 - 0.7$ Gyrs after the onset of star formation in their host galaxies.

The similarity between the SFH parameters of the AGN and the normal galaxies indicates that the AGN do not have a measurable impact on the star formation activity in their host galaxies. In addition, we do not find evidence for a systematic deficit in the cold gas content of the AGN compared to their normal counterparts, which would be expected if feedback from the AGN was depleting the cold gas reservoir in the host galaxies. We conclude that the AGN, in this sample of objects, appear not to be exerting negative feedback on the ISM by removing cold gas and reducing the star formation activity.

While this issue needs to be investigated further, the lack of AGN feedback in the LIRG population may have some intriguing implications for the role of feedback envisaged in galaxy formation models. For example, if we assume that low-redshift LIRGs host similar conditions to star-forming objects at high redshift, then our results imply that obscured AGN in such objects may not significantly affect the star formation in their hosts through e.g. mechanical 'radio-mode' feedback (e.g. Croton et al. 2006). However, both observational (e.g. Nesvadba et al. 2006) and theoretical (e.g. Sijacki et al. 2007) evidence does exist for AGN feedback in the high-redshift galaxy population and indirect evidence for the radio-mode exists in low-redshift *early-type* galaxies (e.g. Best et al. 2005; Schawinski et al. 2007). It is likely, therefore, that conditions in low-redshift LIRGs do not mimic those in the distant Universe ($z > 1$). For example, gas densities at high redshift are expected to be higher[3] and galaxies are likely to be more compact, plausibly allowing the AGN luminosity to couple more effectively to the interstellar material. In addition, galaxies will tend to be less massive, altering the proportional strength of the AGN compared to the potential well of the host galaxy.

Perhaps more intriguing is the fact that (radio-mode) feedback appears to operate in early-type galaxies at low redshift (Schawinski et al. 2007), while it is absent in the low-redshift LIRGs (which are overwhelmingly late-type in terms of their morphologies). Although we have demonstrated that LIRGs that host AGN have prominent bulges, their eye-inspected morphologies show that they are clearly late-type galaxies with a non-negligible disk component. Mechanical feedback from AGN, in the conditions that are prevalent at low redshift (e.g. gas densities, galaxy masses etc), therefore seems to be most efficient in systems which lack a significant disk component.

Finally, we have used the subsample of the LIRG population that exhibits spheroidal or near-spheroidal morphology to explore the properties of 'mixed' major mergers in the local Universe. Early-type systems in our LIRG sample - defined as spheroidal or near-spheroidal objects that are plausible progenitors of elliptical galaxies - have underlying populations that exhibit (SSP-weighted) average ages of ~ 6.9 Gyrs and form between 5 and 30% of their stellar mass in the RSF episode, over time periods between 0.3 and 4 Gyrs (lower limits since most of these objects still show disturbed morphologies). This suggests that these galaxies are the products of 'mixed' major mergers, where at least one of the progenitors has late-type morphology. Mergers between two ellipticals would produce underlying populations that are overwhelmingly old (> 10 Gyrs old) and, since ellipticals are typically gas-poor systems, a 'dry' major merger (or equally a minor merger, see e.g. Figure 1 in Kaviraj et al. 2007d) would not supply enough gas to create the high LIRG-like SFRs in these systems.

The local LIRG population offers a unique window into the vigorous star formation that plausibly shaped much of the galaxy population at high redshift. While these systems are rare at low redshift, an improved understanding of stellar mass assembly in the Universe will be greatly helped by studying the evolution of the LIRG population to high redshift. The advent of deep optical surveys offers an excellent opportunity to extend the analysis presented in this paper by exploiting deep optical photometry to trace the rest-frame UV of galaxy populations at intermediate and high redshifts. In a forthcoming paper, we shall combine deep optical surveys with Spitzer imaging of the Chandra Deep Field-South to quantify the SFHs of distant LIRGs ($0.5 < z < 1.5$) and explore their star formation properties. Combined with this study at low redshift, these results will allow us better understand the evolution of star-forming systems and the interplay between AGN activity and star formation over the last 8-10 billion years of cosmic time.

---

[3] The evolution of the gas density shows a $(1+z)^{3/2}$ dependence with redshift (Rao 1994).

Planck Society, and the Higher Education Funding Council for England. The SDSS Web Site is http://www.sdss.org/.

The SDSS is managed by the Astrophysical Research Consortium for the Participating Institutions. The Participating Institutions are the American Museum of Natural History, Astrophysical Institute Potsdam, University of Basel, University of Cambridge, Case Western Reserve University, University of Chicago, Drexel University, Fermilab, the Institute for Advanced Study, the Japan Participation Group, Johns Hopkins University, the Joint Institute for Nuclear Astrophysics, the Kavli Institute for Particle Astrophysics and Cosmology, the Korean Scientist Group, the Chinese Academy of Sciences (LAMOST), Los Alamos National Laboratory, the Max-Planck-Institute for Astronomy (MPIA), the Max-Planck-Institute for Astrophysics (MPA), New Mexico State University, Ohio State University, University of Pittsburgh, University of Portsmouth, Princeton University, the United States Naval Observatory, and the University of Washington.

GALEX (Galaxy Evolution Explorer) is a NASA Small Explorer, launched in April 2003, developed in cooperation with the Centre National dEtudes Spatiales of France and the Korean Ministry of Science and Technology.

REFERENCES

Adelberger K. L., Steidel C. C., 2000, ApJ, 544, 218
Adelman-McCarthy J. K., SDSS collaboration 2006, ApjS, 162, 38
Alonso M. S., Lambas D. G., Tissera P., Coldwell G., 2007, MNRAS, 375, 1017
Baldwin J. A., Phillips M. M., Terlevich R., 1981, PASP, 93, 5
Bell E. F., Papovich C., Wolf C., Le Floc'h E., Caldwell J. A. R., Barden M., Egami E., McIntosh D. H., Meisenheimer K., Pérez-González P. G., Rieke G. H., Rieke M. J., Rigby J. R., Rix H.-W., 2005, ApJ, 625, 23
Benson A. J., Bower R. G., Frenk C. S., Lacey C. G., Baugh C. M., Cole S., 2003, ApJ, 599, 38
Bernardi M., collaboration S., 2003, AJ, 125, 1882
Best P. N., Kauffmann G., Heckman T. M., Brinchmann J., Charlot S., Ivezić Ž., White S. D. M., 2005, MNRAS, 362, 25
Brinchmann J., Charlot S., White S. D. M., Tremonti C., Kauffmann G., Heckman T., Brinkmann J., 2004, MNRAS, 351, 1151
Buat V., GALEX collaboration 2005, ApJ, 619, L51
Buat V., Marcillac D., Burgarella D., Le Floc'h E., Takeuchi T. T., Iglesias-Paràmo J., Xu C. K., 2007, A&A, 469, 19
Burgarella D., Buat V., Iglesias-Páramo J., 2005b, MNRAS, 360, 1413
Burgarella D. et al. 2005a, ApJ, 619, L63
Calzetti D., Armus L., Bohlin R. C., Kinney A. L., Koornneef J., Storchi-Bergmann T., 2000, ApJ, 533, 682
Calzetti D., Bohlin R. C., Kinney A. L., Storchi-Bergmann T., Heckman T. M., 1995, ApJ, 443, 136
Cao C., Wu H., Wang J.-L., Hao C.-N., Deng Z.-G., Xia X.-Y., Zou Z.-L., 2006, ChJAA, 6, 197
Chakrabarti S., Cox T. J., Hernquist L., Hopkins P. F., Robertson B., Di Matteo T., 2007, ApJ, 658, 840
Chapman S. C., Blain A. W., Ivison R. J., Smail I. R., 2003, Nature, 422, 695
Cowie L. L., Songaila A., Hu E. M., Cohen J. G., 1996, AJ, 112, 839
Croton D. J., Springel V., White S. D. M., De Lucia G., Frenk C. S., Gao L., Jenkins A., Kauffmann G., Navarro J. F., Yoshida N., 2006, MNRAS, 365, 11
De Lucia G., Springel V., White S. D. M., Croton D., Kauffmann G., 2006, MNRAS, 366, 499
Egami E. et al. 2004, ApJS, 154, 130
Elbaz D., Cesarsky C. J., Fadda D., Aussel H., Désert F. X., Franceschini A., Flores H., Harwit M., Puget J. L., Starck J. L., Clements D. L., Danese L., Koo D. C., Mandolesi R., 1999, A&A, 351, L37
Elbaz D., Le Floc'h E., Dole H., Marcillac D., 2005, A&A, 434, L1
Fukugita M., Nakamura O., Turner E. L., Helmboldt J., Nichol R. C., 2004, ApJL, 601, L127
Gao Y., Solomon P. M., 2004a, ApJ
Gao Y., Solomon P. M., 2004b, ApJS
Goto T., 2005, MNRAS, 360, 322
Hopkins A. M., Connolly A. J., Haarsma D. B., Cram L. E., 2001, AJ, 122, 288
Joseph R. D., 1999, Ap&SS, 266, 321
Kauffmann G. et al. 2003a, MNRAS, 346, 1055
Kauffmann G et al. 2003b, MNRAS, 341, 33
Kaviraj S., 2007b, ArXiv:0710.1311, 710
Kaviraj S., Devriendt J. E. G., Ferreras I., Yi S. K., 2005, MNRAS, 360, 60
Kaviraj S., Devriendt J. E. G., Ferreras I., Yi S. K., Silk J., 2006a, MNRAS; astro-ph/0602347
Kaviraj S., Kirkby L. A., Silk J., Sarzi M., 2007c, MNRAS, 382, 960
Kaviraj S., Peirani S., Khochfar S., Silk J., Kay S., 2007d, ArXiv:0711.1493, 711
Kaviraj S., Rey S.-C., Rich R. M., Yoon S.-J., Yi S. K., 2007a, MNRAS, 381, L74
Laag E. A., Canalizo G., van Breugel W., Gates E. L., de Vries W., Stanford S. A., 2006, AJ, 131, 2877
Lilly S. J., Eales S. A., Gear W. K. P., Hammer F., Le Fèvre O., Crampton D., Bond J. R., Dunne L., 1999, ApJ, 518, 641
Lilly S. J., Le Fevre O., Hammer F., Crampton D., 1996, ApJ, 460, L1+
Madau P., della Valle M., Panagia N., 1998, MNRAS, 297, L17+
Martin D. C., GALEX collaboration 2005, ApJ, 619, L1
Melbourne J., Koo D. C., Le Floc'h E., 2005, ApJ, 632, L65
Moshir M., Kopman G., Conrow T. A. O., 1992. Pasadena: Infrared Processing and Analysis Center, California Institute of Technology, 1992, edited by Moshir, M.; Kopman, G.; Conrow, T. a.o.
Nesvadba N. P. H., Lehnert M. D., Eisenhauer F., Gilbert A., Tecza M., Abuter R., 2006, ApJ, 650, 693
Neugebauer G. et al. 1984, ApJ, 278, L1
Rao S. M., 1994, PhD thesis, AA(Pittsburgh Univ.)
Rowan-Robinson M., Crawford J., 1989, MNRAS, 238, 523
Sanders D., Ishida C., 2004, in Aalto S., Huttemeister S., Pedlar A., eds, The Neutral ISM in Starburst Galaxies Vol. 320 of Astronomical Society of the Pacific Conference Series. pp 230–+

Sanders D. B., 1999, AP&SS, 266, 331

Sanders D. B., 2003, Journal of the Korean Astronomical Society, 36, 149

Sanders D. B., Mirabel I. F., 1996, ARA&A, 34, 749

Schawinski K., Thomas D., Sarzi M., Maraston C., Kaviraj S., Joo S.-J., Yi S. K., Silk J., 2007, MNRAS, 382, 1415

Seibert et al. 2005, ApJ, 619, L23

Sijacki D., Springel V., di Matteo T., Hernquist L., 2007, MNRAS, 380, 877

Silk J., 2005, MNRAS, 364, 1337

Silk J., Rees M. J., 1998, A&A, 331, L1

Silva L., Maiolino R., Granato G. L., 2004, MNRAS, 355, 973

Smail I., Ivison R. J., Blain A. W., 1997, ApJ, 490, L5+

Soifer B. T., Neugebauer G., 1991, AJ, 101, 354

Soifer B. T., Neugebauer G., Helou G., Lonsdale C. J., Hacking P., Rice W., Houck J. R., Low F. J., Rowan-Robinson M., 1984, ApJ, 283, L1

Soifer B. T., Sanders D. B., Madore B. F., Neugebauer G., Danielson G. E., Elias J. H., Lonsdale C. J., Rice W. L., 1987, ApJ, 320, 238

Strateva I. et al. 2001, AJ, 122, 1861

Strauss et al. 2002, AJ, 124, 1810

Taniguchi Y., Cowie L. L., Sato Y., Sanders D. B., Kawara K., Joseph R., Okuda H., Wynn-Williams C. G., Matsumoto T., Chambers K. C., Wakamatsu K., Desert F. X., Sofue Y., Matsuhara H., 1997, A&A, 328, L9

Teng S. H., Wilson A. S., Veilleux S., Young A. J., Sanders D. B., Nagar N. M., 2005, ApJ, 633, 664

Tremonti C. A., Heckman T. M., Kauffmann G., Brinchmann J., Charlot S., White S. D. M., Seibert M., Peng E. W., Schlegel D. J., Uomoto A., Fukugita M., Brinkmann J., 2004, ApJ, 613, 898

van Dokkum P. G., 2005, AJ, 130, 2647

Veilleux S., Sanders D. B., Kim D.-C., 1999, ApJ, 522, 139

Wang B., Heckman T. M., 1996, ApJ, 457, 645

Wang J. L., Xia X. Y., Mao S., Cao C., Wu H., Deng Z. G., 2006, ApJ, 649, 722

Worthey G., 1994, ApJS, 95, 107

Wyder T. K. et al. 2007, ApJS, 173, 293

Yi S. K., 2003, ApJ, 582, 202

Zauderer B. A., Veilleux S., Yee H. K. C., 2007, ApJ, 659, 1096

Zheng X. Z., Hammer F., Flores H., Assémat F., Pelat D., 2004, A&A, 421, 847